Hydration and hydrogen bond network of water around hydrophobic surface investigated by terahertz spectroscopy.

AUTHOR(S):

Shiraga, K; Suzuki, T; Kondo, N; Ogawa, Y

CITATION:

Shiraga, K ...[et al]. Hydration and hydrogen bond network of water around hydrophobic surface investigated by terahertz spectroscopy.. The Journal of chemical physics 2014, 141(23): 235103.

ISSUE DATE:

2014-12-21

URL:

http://hdl.handle.net/2433/193257

Hydration and hydrogen bond network of water around hydrophobic surface investigated by terahertz spectroscopy

K. Shiraga, T. Suzuki, N. Kondo, and Y. Ogawa

Citation: The Journal of Chemical Physics **141**, 235103 (2014); doi: 10.1063/1.4903544
View online: http://dx.doi.org/10.1063/1.4903544
View Table of Contents: http://scitation.aip.org/content/aip/journal/jcp/141/23?ver=pdfcov
Published by the AIP Publishing

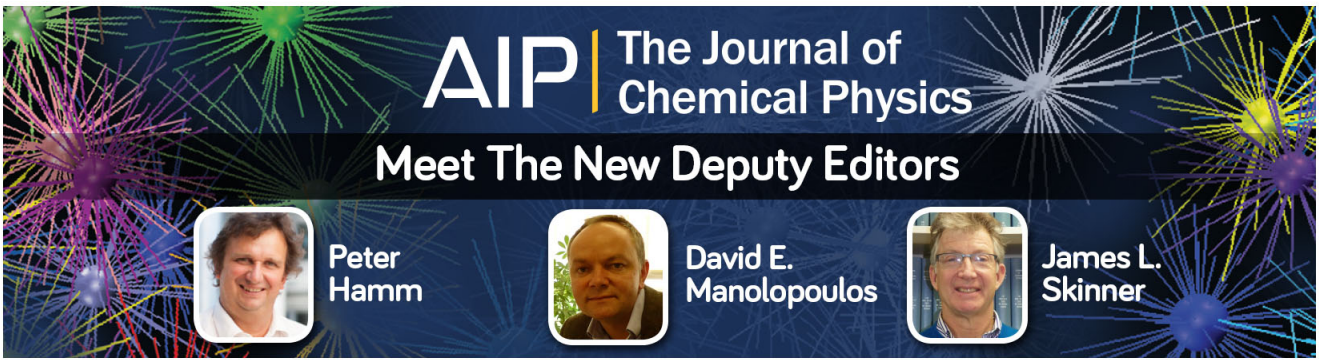

THE JOURNAL OF CHEMICAL PHYSICS **141**, 235103 (2014)

Hydration and hydrogen bond network of water around hydrophobic surface investigated by terahertz spectroscopy

K. Shiraga, T. Suzuki, N. Kondo, and Y. Ogawa[a)]
Graduate School of Agriculture, Kyoto University, Kitashirakawa-oiwakecho, Sakyo-ku, Kyoto 606-8502, Japan

(Received 10 September 2014; accepted 25 November 2014; published online 16 December 2014)

Water conformation around hydrophobic side chains of four amino acids (glycine, L-alanine, L-aminobutyric acid, and L-norvaline) was investigated via changes in complex dielectric constant in the terahertz (THz) region. Each of these amino acids has the same hydrophilic backbone, with successive additions of hydrophobic straight methylene groups (–CH_2–) to the side chain. Changes in the degree of hydration (number of dynamically retarded water molecules relative to bulk water) and the structural conformation of the water hydrogen bond (HB) network related to the number of methylene groups were quantitatively measured. Since dielectric responses in the THz region represent water relaxations and water HB vibrations at a sub-picosecond and picosecond timescale, these measurements characterized the water relaxations and HB vibrations perturbed by the methylene apolar groups. We found each successive straight –CH_2– group on the side chain restrained approximately two hydrophobic hydration water molecules. Additionally, the number of non-hydrogen-bonded (NHB) water molecules increased slightly around these hydrophobic side chains. The latter result seems to contradict the iceberg model proposed by Frank and Evans, where water molecules are said to be more ordered around apolar surfaces. Furthermore, we compared the water–hydrophilic interactions of the hydrophilic amino acid backbone with those with the water–hydrophobic interactions around the side chains. As the hydrophobicity of the side chain increased, the ordering of the surrounding water HB network was altered from that surrounding the hydrophilic amino acid backbone, thereby diminishing the fraction of NHB water and ordering the surrounding tetrahedral water HB network. © *2014 AIP Publishing LLC*. [http://dx.doi.org/10.1063/1.4903544]

I. INTRODUCTION

Interactions of water with hydrophobic groups play an essential role in orchestrating molecular-scale phenomena in living systems, such as protein conformation,[1] lipid self-assembly,[2] and binding in the ligand.[3] Thermodynamical studies have shown that when a hydrophobic solute is dissolved in water, the hydrogen bonds (HBs) of the water molecules in the first coordination layer surrounding a hydrophobic solute are disrupted thereby creating a void. In order to minimize any enthalpic penalty associated with the breaking of these HBs, water molecules are forced to reorient in a more favorable direction to avoid breaking HBs.[4–7]

From a thermodynamic point of view, this ends up in significantly decreasing the entropy (ΔS) of the surrounding HB network and also slightly decreasing the enthalpy (ΔH).[5,6] Furthermore, water interactions surrounding the hydrophobic group also induce an increase in the heat capacity (C_p). This increase in C_p, and the large negative change in ΔS, is associated with a so-called "hydrophobic hydration" phenomena, where the HBs are strengthened and tetrahedral structure of the surrounding water undergoes "ordering" around the hydrophobic solute.[7]

To characterize the thermodynamics of hydrophobic hydration, Frank and Evans proposed an "iceberg" model, where the water takes on a frozen or immobilized patch like structure, almost a microscopic ice-like formation, around the hydrophobic groups.[8] While, Head-Gordon *et al.* described the hydrophobic hydration water as forming planar pentagon rings that extend for two layers,[9] similar to natural gas clathrates, rather than hexagonal rings of ice.[10]

These explanations of the static structure of water surrounding hydrophobic groups, which have been criticized,[11] do not, however, provide information regarding the dynamical aspects of the water – hydrophobic group interactions. Although the iceberg model is appealing in terms of a static structure, in the dynamical aspects this model has been questioned, with few experimental or computational results to support the model.[12] Other more recent experimental results suggest a dynamically "moderate" view of the iceberg model:[13–15] water around the apolar groups is actually ordered with slow reorientational dynamics, but the degree of rotational slowdown at ambient conditions is at most a factor of 2 compared to that of bulk water (not as pronounced as "ice"). The reorientational slowdown can be ascribed to a solute excluded volume effect, in which some of the water molecules are hindered from finding new HB partners around the hydrophobic solute, moderately retarding the HB exchange rate.[14]

On the other hand, experimental studies, such as NMR,[13] time-resolved IR spectroscopy,[15,16] X-ray/neutron diffraction[17,18] and dielectric spectroscopy in the GHz

a)Author to whom correspondence should be addressed. Electronic mail: ogawayu@kais.kyoto-u.ac.jp. Fax: +81 75 753 6171.

region[19,20] and MD simulations,[21–23] have been used to investigate the dynamical and structural properties of water surrounding hydrophobic groups. X-ray/neutron diffraction and MD simulations have been mainly used to explore the "static" structure of water around apolar solutes via a radial distribution function (RDF). Whereas, NMR and dielectric spectroscopy directly reflect the rotational dynamics of the hydrated water surrounding the hydrophobic groups, and can be used to quantitatively determine the hydration number and the retardation factor with respect to bulk water. In addition, time-resolved IR spectroscopy has been used to infer the reorientational dynamics of water from the anisotropy decay of the intramolecular OH stretching vibration. Thus, these studies focus on the retardation dynamics of hydrophobic hydration and the elongated lifetime of the HB. However, to achieve a more wholistic picture, such details need to be explained within the context of what is happening in the surrounding HB network of water, since most of the unique physical properties of water originate from their HB structures and dynamics.[24,25]

While the dynamical structures of HBs have been estimated, no consensus of what is happening to the HBs around the hydrophobic solute has been achieved. This is in part due to the fact that no "direct" probe of water HB dynamics has been available to date. Such a situation can be attributed to the pico- to sub-picosecond lifetimes of HBs,[26] which are too short for the NMR and dielectric spectroscopy time window. It is certain that time-resolved IR spectroscopy can record time-dependent change at the pico- to sub-picosecond timescales, but estimating intermolecular HB dynamics of water from intramolecular OH stretching vibration would be still "indirect" since the resonance lifetime of OH stretching (∼10 fs) is much shorter than the HB lifetime. Fortunately, recent advances in terahertz (THz) spectroscopy may allow us to directly observe these HB dynamics, since the oscillation period of the THz waves is on a picosecond and sub-picosecond timescale.[27–29] This means that dielectric responses in the THz region are selectively sensitive to the HB dynamics of water, such as the reorientations of bulk water and HB stretching, with negligible interference from apolar solutes and hydrated water relaxation (typically in the low GHz region) and intramolecular dipole fluctuations (at higher frequencies). These unique aspects of THz spectroscopy have recently been used to quantitatively measure hydration state,[30] the existence of non-hydrogen-bonded (NHB) water[28] and the tetrahedral ordering of the water HB network.[29] However, attempts to discuss water–hydrophobic group interactions in aqueous solutions have yet to be examined systematically using THz spectroscopy.

In this study, THz spectroscopy over a broad frequency range was used to determine the complex dielectric constant ($\tilde{\varepsilon} = \mathrm{Re}[\varepsilon] - i\mathrm{Im}[\varepsilon]$) of amino acid solutions with increasing the number of methylene (–CH_2–) groups in the side chain. Amino acid solutions provide a convenient platform to explore hydrophobicity, since they all contain the same hydrophilic backbone, while the hydrophobicity of the side chain can be successively increased. In our experiments water–hydrophobic group interactions were examined in terms of (a) hydration number, (b) the population of solute-induced NHB water, and (c) the tetrahedral water ordering engaged in the HB network.

II. METHOD

A. Sample preparation

Powder samples of glycine (Gly), L-alanine (Ala), L-aminobutyric acid (Aba), and L-norvaline (*n*-Val) were purchased from Wako Pure Chemical Ind., Ltd. and dissolved into distilled water to prepare 50 mg/ml solutions without further purification. The neutral molecular structures of these amino acids are depicted in Figure 1. However, the –COOH group is deprotonated and the $–NH_2$ group is protonated, thus yielding a zwitterion state with anionic and cationic groups: $–COO^-$ and $–NH_3^+$ in aqueous solution. In such a zwitterion state under the isoelectric point (around pH = 6 for all the investigated amino acids), amino acids behave in their native roles that are relevant to biological functions.

B. Complex dielectric constant measurements

1. Terahertz time-domain attenuated total reflection spectroscopy

In order to detect tiny changes induced by water–hydrophobic group interactions in the amino acid solutions, complex dielectric constants between 0.2 and 3.0 THz were measured by a THz time-domain attenuated total reflection (THz TD-ATR) spectrometer, TAS7500 (Advantest Co., Ltd.), where the incident angle is 57° and silicon is used as an ATR prism. A temperature controller was attached to the ATR prism to keep sample temperature at 300 ± 0.1 K. In this time-domain measurement scheme, a temporal THz waveform is recorded with and without a sample. The temporal THz waveform with the sample undergoes both an amplitude decrease and time delay compared to that without the sample. By Fourier transforming the time-domain THz waveform into the frequency-domain spectrum, we can simultaneously obtain both the reflectance $R(\omega)$ and phase shift spectrum $\varphi(\omega)$. Therefore, from these two parameters the real part $\mathrm{Re}[\varepsilon(\omega)]$ and imaginary part $\mathrm{Im}[\varepsilon(\omega)]$ of the complex dielectric constants can be calculated directly. The detailed calculation procedures to determine the complex dielectric constants are explained in Refs. 31 and 32.

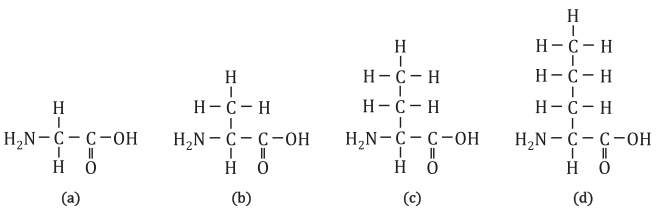

FIG. 1. The molecular structure of neutral amino acids. (a) Glycine, (b) Alanine, (c) Aminobutyric acid, (d) Norvaline.

2. Far-infrared Fourier transform attenuated total reflection spectroscopy

In the higher frequency region up to 12 THz, we measured the reflectance spectrum $R(\omega)$ by far-infrared Fourier transform attenuated total reflection (FIR FT-ATR) spectroscopy. Unlike time-domain spectroscopy, FT spectroscopy directly records the frequency-domain spectrum and thus only the reflectance $R(\omega)$ is measured. To determine the complex dielectric constants, the Kramers-Kronig relation, along with the procedure proposed by Bertie and Lan,[33] was used to theoretically calculate the phase shift spectrum $\varphi(\omega)$,

$$\varphi(\omega) = -\frac{2}{\pi}\int_0^{\omega_u} \frac{\omega_a \ln\sqrt{R(\omega_a)}}{{\omega_a}^2 - \omega^2} d\omega_a + \varphi_\infty, \quad (1)$$

where ω_u is the upper integration limit and φ_∞ represents the phase shift at $\omega = \omega_u$. Equation (1) is identical for both *s*- and *p*-polarizations. Though the first term in Eq. (1) is calculated by the experimental result, $R(\omega)$, the second term (φ_∞) cannot be directly determined from our measurement.[34] To overcome this problem, we set φ_∞ as the value that best fits the THz TD-ATR measurement result between 2.8 and 3.2 THz, so as to smoothly connect the THz TD-ATR and FIR FT-ATR results. In our FIR FT-ATR measurements, a FARIS-1s spectrometer (Jasco Co.), in which the incident angle is 45° and silicon ATR prism with a temperature controller was used. A ceramic heater and pyroelectric element (deuterated triglycine sulfate: DTGS) were chosen as a light source and detector, respectively. Since the ceramic heater radiates unpolarized electromagnetic waves, experimentally measured reflectance $R(\omega)$ is composed of both *s*- and *p*-polarization components. When the incident light undergoes only one reflection at the incident angle of 45°, we obtain

$$R(\omega) = \frac{R_s(\omega) + R_p(\omega)}{2} = \frac{R_s(\omega) + {R_s}^2(\omega)}{2}, \quad (2)$$

where subscription s and p represents *s*- and *p*-polarization, respectively.[33] Hence, we can calculate the $R_s(\omega)$ from the unpolarized reflectance spectrum $R(\omega)$. After deriving $\varphi_s(\omega)$ by Eq. (1), the Fresnel's reflection coefficient for *s*-polarization $\tilde{r}_s(\omega)$ is associated with the complex dielectric constant of the sample, $\tilde{\varepsilon}_2(\omega)$ by the following equation:

$$\tilde{r}_s(\omega) = R_s(\omega)\exp[-i\varphi_s(\omega)] = \frac{\sqrt{\varepsilon_1(\omega)}\cos\theta - \sqrt{\tilde{\varepsilon}_2(\omega)}\sqrt{1 - \frac{\varepsilon_1(\omega)}{\tilde{\varepsilon}_2(\omega)}\sin^2\theta}}{\sqrt{\varepsilon_1(\omega)}\cos\theta + \sqrt{\tilde{\varepsilon}_2(\omega)}\sqrt{1 - \frac{\varepsilon_1(\omega)}{\tilde{\varepsilon}_2(\omega)}\sin^2\theta}}, \quad (3)$$

where $\varepsilon_1(\omega)$ and θ is the dielectric constant of the ATR prism and the incident angle, respectively.

3. Standard errors of measurements

Since the TAS7500 exhibits better signal-to-noise ratios at lower frequencies, the standard errors in the real and imaginary part of the complex dielectric constant ($\tilde{\varepsilon}_{SE}$) below 1 THz were less than 0.020 and 0.025 (corresponding to ~0.3% and ~0.4%), respectively. Even in the higher frequency region between 1 and 3 THz, where the signal-to-noise ratio is not as good as in the low frequency region, the standard errors were no more than 0.090 (corresponding to 2.5%) in the real part and 0.045 (3.0%) in the imaginary part.

The FARIS-1s spectrometer has a relatively consistent accuracy over the investigated frequency region (3–12 THz), exhibiting standard errors of reflectance $R(\omega)$ smaller than 0.4%. After the Kramers-Kronig transform, $\tilde{\varepsilon}_{SE}$ in the real and imaginary part was: 0.035 and 0.045 (corresponding to 1.4% and 2.5%) at 5 THz and 0.040 and 0.015 (1.8% and 1.5%) at 10 THz, respectively.

The values listed above hold for both distilled water and the amino acid solutions, indicating the measured complex dielectric constants are accurate enough for further analysis.

III. RESULTS AND DISCUSSIONS

A. Data analysis

The measured complex dielectric constants from 0.2 to 12 THz of the distilled water and 50 mg/ml glycine solution (as a representative of the four examined amino acids) were plotted in Fig. 2. Although there were slight deviations between the distilled water and glycine solution, the frequency dispersion of the glycine solution was quite similar to that of the distilled water. These observations reconfirm that the dielectric responses in the THz region are particularly sensitive to water. Furthermore, no specific absorption bands of glycine crystal[35] were observed. This is because the glycine–glycine intermolecular vibration modes will be disappeared in the aqueous solution where the glycine solutes are dispersed and surrounded by water molecules. Similar tendencies were also observed for the other three amino acid solutions (data

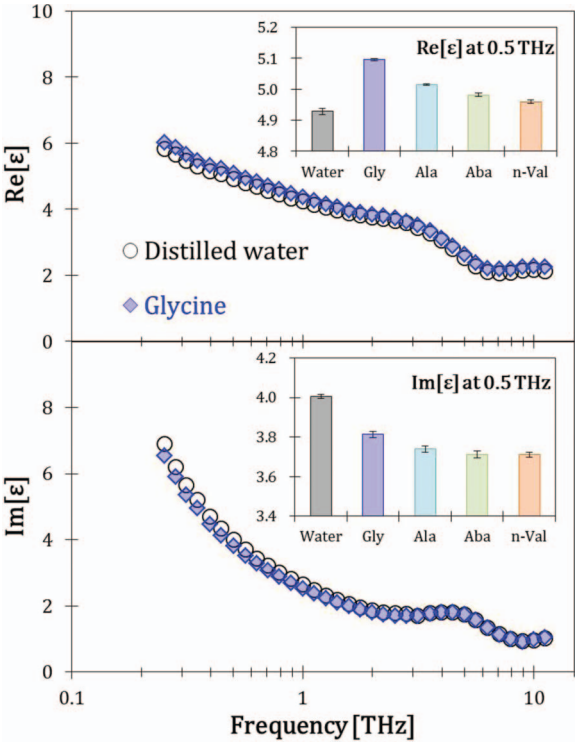

FIG. 2. (Upper) real part and (lower) imaginary part of the complex dielectric constant of distilled water (black circle) and glycine (blue triangle). The insets show the comparison at 0.5 THz with error bars.

not shown). In the insets in Fig. 2, the complex dielectric constant at 0.5 THz was shown to confirm the representative trend over this frequency range. Both real and imaginary parts were statistically distinguished among the amino acid solutions, indicating each amino acid interact with water in a different manner or in a different magnitude.

Since the frequency region between 0.2 and 12 THz corresponds to the 0.01–0.8 ps time window, the complex dielectric constants in this region correspond to dipolar fluctuations (such as reorientation and vibrations) at these timescales. Recent dielectric spectroscopy in the GHz region has revealed that three reorientation dynamics contribute to the complex dielectric constant of amino acid solutions between 0.1 and 89 GHz:[36,37] the reorientation of hydrated amino acids, hydrogen-bonded bulk water (HB bulk water), and non-hydrogen-bonded bulk water (NHB bulk water). Of these three reorientation dynamics, only the latter two are responsive above 0.2 THz, meaning the reorientational motions of hydrated amino acids will not be detected in the measurement window of this study.[35–37] Additionally, it should be noted that the HB bulk water and NHB bulk water can be distinguished by their dielectric responses, since the NHB water reorients faster than the HB water by an order of magnitude.[28] These water reorientation dynamics are described as Debye-type relaxation modes. Moreover, at higher frequencies two damped Lorentzian-type vibration modes are found around 5 and 15 THz for distilled water.[28,29] These vibrations are assigned to an intermolecular stretching mode and intermolecular libration mode of water, respectively. As such, they directly reflect the HB dynamics of water and thus are sensitive to the dynamical structure of the HB network and the HB strength.[12,38] These intermolecular stretch and libration modes undergo a slight peak shift and/or broadening, which comes from the modulation of the HB ordering and/or strength.

Thereby, the complex dielectric constants from 0.2 to 12 THz are selectively associated with reorientational and vibrational dynamics of the water HB network, since the direct influence of amino acid solutes can be neglected. Consequently, complex dielectric constants $\tilde{\varepsilon}(\omega)$ between 0.2 and 12 THz are a superposition of theoretical complex susceptibilities $\tilde{\chi}(\omega)$; the slow relaxation $\tilde{\chi}_{\mathrm{slow}}(\omega)$ (reorientation of HB bulk water), fast relaxation $\tilde{\chi}_{\mathrm{fast}}(\omega)$ (reorientation of NHB bulk water), intermolecular stretching vibration $\tilde{\chi}_{\mathrm{S}}(\omega)$, intermolecular libration $\tilde{\chi}_{\mathrm{L}}(\omega)$, and higher frequency limit ε_{∞}. As pointed out by Yada *et al.*,[28] two Lorentzian-type vibration modes are imperative to accurately describe the dielectric responses in the THz region, avoiding the uncertainty of the Debye relaxation components.[28] Then, the experimental result $\tilde{\varepsilon}(\omega)$ can be fitted to the following equation:

$$\begin{aligned}\tilde{\varepsilon}(\omega) &= \tilde{\chi}_{\mathrm{slow}}(\omega) + \tilde{\chi}_{\mathrm{fast}}(\omega) + \tilde{\chi}_{\mathrm{S}}(\omega) + \tilde{\chi}_{\mathrm{L}}(\omega) + \varepsilon_{\infty} \\ &= \frac{\Delta\varepsilon_{\mathrm{slow}}}{1 + i\omega\tau_{\mathrm{slow}}} + \frac{\Delta\varepsilon_{\mathrm{fast}}}{1 + i\omega\tau_{\mathrm{fast}}} + \frac{\Delta V_{\mathrm{S}}{\omega_{\mathrm{S}}}^2}{{\omega_{\mathrm{S}}}^2 - \omega^2 + i\omega\gamma_{\mathrm{S}}} \\ &\quad + \frac{\Delta V_{\mathrm{L}}{\omega_{\mathrm{L}}}^2}{{\omega_{\mathrm{L}}}^2 - \omega^2 + i\omega\gamma_{\mathrm{L}}} + \varepsilon_{\infty}, \end{aligned} \tag{4}$$

where $\Delta\varepsilon_{\mathrm{slow(fast)}}$ is the relaxation strength, $\tau_{\mathrm{slow(fast)}}$ is the relaxation time, $\Delta V_{\mathrm{S(L)}}$ is the vibration strength, $\omega_{\mathrm{S(L)}}$ is the resonant frequency, and $\gamma_{\mathrm{S(L)}}$ is the damping constant. In the present analysis, the experimentally determined $\tilde{\varepsilon}(\omega)$, including the experimental standard errors, were decomposed into these theoretical susceptibilities by a least square method until the chi-square value of the Levenberg–Marquardt algorithm[39] satisfies $<10^{-9}$. For a successful fit, the relaxation time of the slow relaxation mode at 300 K was fixed at $\tau_{\mathrm{slow}} = 7.93$ ps, according to the critical slowing formula of water.[40] This formula was originally applied to pure water, but is assumed to be valid for the amino acid solutions since it has been confirmed that τ_{slow} is unchanged even in the presence of solute molecules.[36,41] The fitted parameters as well as the standard deviations of the distilled water ($\Delta\varepsilon_{\mathrm{slow}} = 72.06 \pm 0.39$, $\Delta\varepsilon_{\mathrm{fast}} = 2.02 \pm 0.04$, $\tau_{\mathrm{fast}} = 271 \pm 24$ fs, $\Delta V_{\mathrm{S}} = 1.24 \pm 0.04$, $\omega_{\mathrm{S}} = 5.22 \pm 0.05$ THz/2π, $\gamma_{\mathrm{S}} = 5.31 \pm 0.09$ THz/2π, $\Delta V_{\mathrm{L}} = 0.49 \pm 0.12$, $\omega_{\mathrm{L}} = 13.91 \pm 0.26$ THz/2π, and $\gamma_{\mathrm{L}} = 7.70 \pm 0.28$ THz/2π) are in good accordance with previous studies by Yada *et al.* (at 293 and 296 K).[28,29] Here, it should be noted that these standard deviations are not solely a result of the fitting procedure of the "average" $\tilde{\varepsilon}(\omega)$. Concretely, each experimental result $\tilde{\varepsilon}(\omega)$ was substituted into the left-hand side of Eq. (4) and the resulting spread in the fitting parameters were considered as the standard deviations of the fitting procedure.

The fitted versus the experimental results for the 50 mg/ml glycine solution are shown in Fig. 3. The

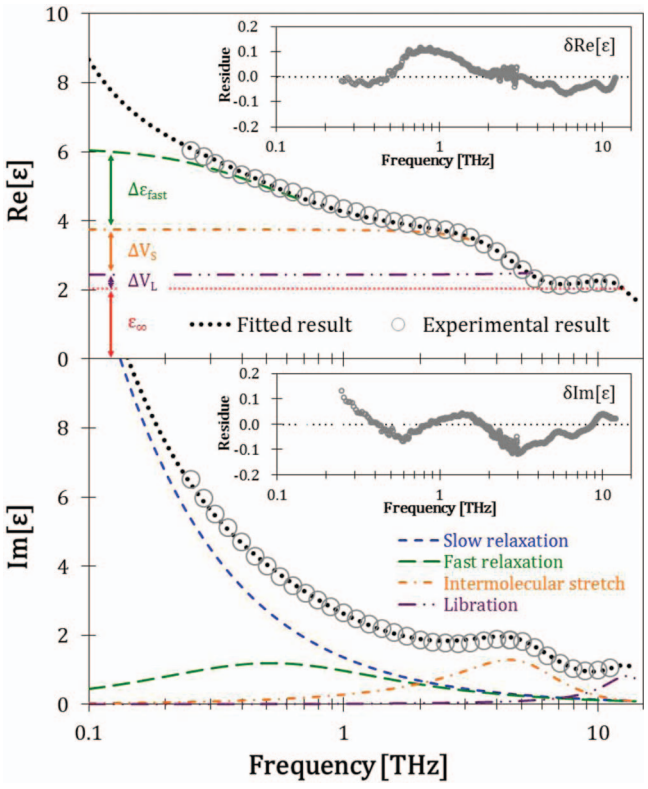

FIG. 3. Decomposition of the complex dielectric constant of glycine solution into theoretical susceptibilities; slow relaxation (blue broken line), fast relaxation (green long broken line), intermolecular stretch vibration (orange chain line), libration (purple two-dot chain line), and high-frequency limit (red dot line). The fitted result was represented as the sum of the five complex susceptibilities. The insets show the fitting residues, $\delta\mathrm{Re}[\varepsilon] = \mathrm{Re}[\varepsilon_{\mathrm{exp}}] - \mathrm{Re}[\varepsilon_{\mathrm{fit}}]$ and $\delta\mathrm{Im}[\varepsilon] = \mathrm{Im}[\varepsilon_{\mathrm{exp}}] - \mathrm{Im}[\varepsilon_{\mathrm{fit}}]$.

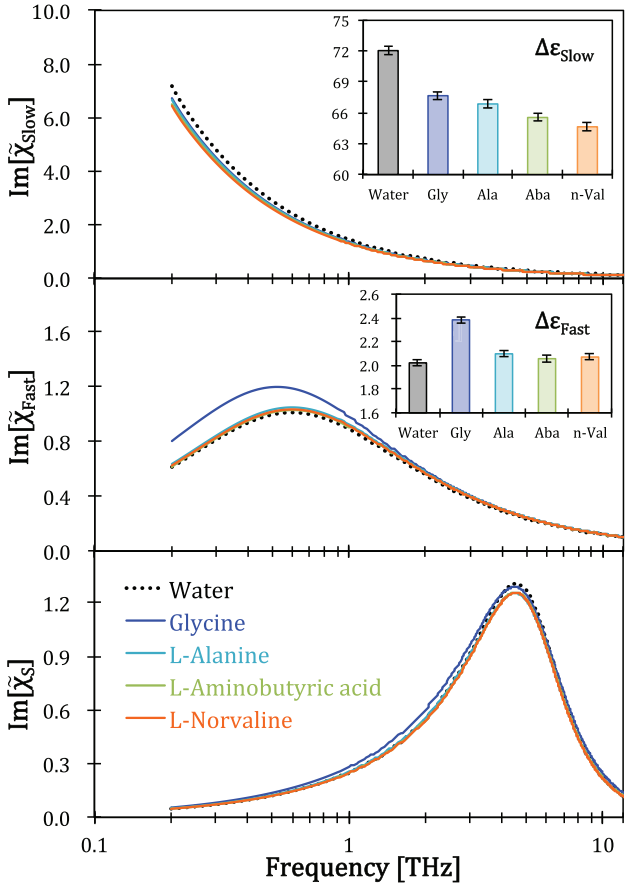

FIG. 4. The comparison in the calculated imaginary part of the complex susceptibilities of the distilled water and amino acid solutions: (upper) slow relaxation, (middle) fast relaxation, and (lower) intermolecular stretching vibration mode. These imaginary parts are the theoretical results calculated from Eq. (4). The insets show the solute-dependent relaxations strength, with standard errors arising from the fitting procedure.

residues according to the fitting procedure, $\delta\tilde{\varepsilon}(\omega) = \tilde{\varepsilon}_{\text{exp.}}(\omega) - \tilde{\varepsilon}_{\text{fit.}}(\omega)$, where $\tilde{\varepsilon}_{\text{exp.}}(\omega)$ and $\tilde{\varepsilon}_{\text{fit.}}(\omega)$ are the complex dielectric constants of the experiment (left hand side of Eq. (4)) and the fitting (right hand side of Eq. (4)), were within ± 0.1, validating the fitting function as represented in Eq. (4). Therefore, based on the best-fitted free parameters ($\Delta\varepsilon_{\text{slow}}$, $\Delta\varepsilon_{\text{fast}}$, τ_{fast}, ΔV_{S}, ω_{S}, and γ_{S}) for each sample, detailed discussions are to be made in Secs. III B–III D. Additionally, the calculated imaginary susceptibilities of the distilled water and all the amino acid solutions obtained by the fitting procedure are compared in Fig. 4, and the solute-dependent relaxation strengths ($\Delta\varepsilon_{\text{slow}}$ and $\Delta\varepsilon_{\text{fast}}$) are shown in the insets. While $\tilde{\chi}_{\text{fast}}(\omega)$ exhibits a small but clear peak around 0.5 THz, $\tilde{\chi}_{\text{slow}}(\omega)$ was monotonously decreased above 0.2 THz since the THz region lies in the high frequency tail of the slow relaxation mode peaked around 0.02 THz. For the intermolecular stretching vibration mode of water, $\tilde{\chi}_{\text{S}}(\omega)$, a slight attenuation, peak shift, and broadening can be observed. This originates from modulations in the water HB network induced by the amino acid solutes. Note that the intermolecular libration mode of water, $\tilde{\chi}_{\text{L}}(\omega)$, will not be discussed in detail here since the absorption peak (~15 THz) is outside the measured range.

B. Hydration states in amino acid solutions

We will first focus on the hydration number followed by the fraction of NHB bulk water released from the HB network (Sec. III C) via estimates of the slow and fast relaxation of bulk water molecules. Although the relaxation mode of hydrated water is outside the THz region, we can indirectly estimate the hydration state from the reduced volume fraction of bulk water.[30] The slow relaxation mode in the imaginary part exhibited a decrease for all the amino acids compared to distilled water (Fig. 4). Since $\Delta\varepsilon_{\text{slow}}$ is proportional to the number of HB bulk water molecules, these results indicate the volume fraction of HB bulk water was reduced in the amino acid solutions compared to that in distilled water. This reduction in $\Delta\varepsilon_{\text{slow}}$ can be explained by three factors: (1) A part of the volume of the HB bulk water is replaced by amino acid solutes (= water dilution), (2) HB bulk water that is captured by a solute molecule is dynamically retarded when it becomes hydrated water (= hydration effect), and (3) amino acids disturb the water HBs and thus release NHB bulk water from the HB network (= destructuring effect). In order to selectively understand the hydration effect removing the excess influence of water dilution and destructuring effect, we estimated the hydration number, where hydrated water is defined as the water molecules that are dynamically slowed down and not detectable in the THz region. In this case, the bulk water molar concentration in the solution (C_{bulk}) is calculated by[41]

$$C_{\text{bulk}} = \frac{\Delta\varepsilon^{\text{s}}_{\text{slow}} + \Delta\varepsilon^{\text{s}}_{\text{fast}}}{\Delta\varepsilon^{\text{w}}_{\text{slow}} + \Delta\varepsilon^{\text{w}}_{\text{fast}}} \frac{\rho_{\text{w}}}{M_{\text{w}}}, \tag{5}$$

where $\Delta\varepsilon^{\text{s(w)}}$ represents the relaxation strength of solution (distilled water), ρ_{w} is density of water, and M_{w} is molecular weight of water. Then, the law of error-propagation was used to determine the errors in the bulk water concentration ($C_{\text{bulk}} \pm \delta C_{\text{bulk}}$) by substituting $\Delta\varepsilon^{\text{s}}_{\text{slow}} \pm \delta\Delta\varepsilon^{\text{s}}_{\text{slow}}$, $\Delta\varepsilon^{\text{s}}_{\text{fast}} \pm \delta\Delta\varepsilon^{\text{s}}_{\text{fast}}$, $\Delta\varepsilon^{\text{w}}_{\text{slow}} \pm \delta\Delta\varepsilon^{\text{w}}_{\text{slow}}$, and $\Delta\varepsilon^{\text{w}}_{\text{fast}} \pm \delta\Delta\varepsilon^{\text{w}}_{\text{fast}}$ into $\Delta\varepsilon^{\text{s}}_{\text{slow}}$, $\Delta\varepsilon^{\text{s}}_{\text{fast}}$, $\Delta\varepsilon^{\text{w}}_{\text{slow}}$ and $\Delta\varepsilon^{\text{w}}_{\text{fast}}$ in Eq. (5), respectively, where $\delta\Delta\varepsilon$ is the standard deviation of the fitting procedure. Given C_{water} and C denote the "stoichiometric" molar concentration of water and solute in the system, we can deduce the hydration number n_{hyd} per a solute from Eq. (6),[41]

$$n_{\text{hyd}} = \frac{C_{\text{water}} - C_{\text{bulk}}}{C}. \tag{6}$$

By substituting C_{bulk} in Eq. (6) into $C_{\text{bulk}} \pm \delta C_{\text{bulk}}$, the errors in n_{hyd} were determined. The "stoichiometric" water molar concentration (C_{water}) was determined from the density measurement of the amino acid solutions (see Table I). For all the amino acid solutions, C_{water} was smaller than that of distilled water (= 55.55 mol/l) due to a water dilution effect, and therefore, the hydration number was determined without obstruction of the factor (1) (= water dilution). Furthermore, since both C_{water} and C_{bulk} contain exactly same amount of NHB bulk water, $C_{\text{water}} - C_{\text{bulk}}$ cancels out the influence of the factor (3) (= destructuring effect).

The hydration number n_{hyd} and molarity of hydrated water ($C_{\text{hyd}} = C_{\text{water}} - C_{\text{bulk}}$) are summarized in Table I. Additionally, the relationship between the amino acid SASA (solvent accessible surface area)[20] and n_{hyd} are shown in Fig. 5.

TABLE I. Classification of water in amino acid solutions.

	Water	Gly	Ala	Aba	*n*-Val
SASA (Å^2) [a]	...	226.7	249.5	275.5	306.0
Hydrophobicity π [b]	...	0.00	0.31	0.82	1.37
Density (g/ml)	...	1.019 ± 0.005	1.013 ± 0.007	1.012 ± 0.002	1.009 ± 0.002
n_{hyd} (/solute)	...	1.90	3.17	5.65	7.60
n_{NHB} (/solute)	...	0.53	0.29	0.33	0.44
C_{water} (mol/l)	55.55	53.81	53.50	53.44	53.28
C_{bulk} (mol/l)	55.55	52.54	51.72	50.71	50.04
C_{HB} (mol/l)	54.04	50.75	50.15	49.16	48.48
C_{NHB} (mol/l)	1.58	1.79	1.57	1.54	1.55
C_{hyd} (mol/l)	...	1.27	1.78	2.74	3.24

[a]Literature values cited from Ref 20. SASA stands for solvent accessible surface area, when a oxygen radius of 1.4 Å, a nitrogen radius of 1.55 Å, and a carbon radius of 2.0 Å.
[b]Citation from Ref 50. Hydrophobicity of the amino acid side chain (π) is calculated by the equation: $\pi = \log P$(amino acid) $- \log P$(glycine), where P is the partition coefficient of the amino acid and of glycine in octanol/water.[43]

Although a linear positive correlation was observed, it should be noted that both hydrophobic hydration and hydrophilic hydration are counted as hydration water (except for glycine, where hydrated water is entirely originated from hydrophilic nature of polar groups in the amino acid backbone; while the other three amino acids have additional hydrophobic side chains, $-CH_2-$).

Our estimate of n_{hyd}(gly) = 1.9 represents the hydrophilic hydration capacity of the amino acid backbone. In zwitterions, the $-NH_3^+$ and $-COO^-$ groups separate in space to create a pronounced molecular dipole moment; facilitating the coupling to polar solvents, such as water.[42] From a thermodynamical point of view, the $-COO^-$ group is a "structure-maker," while the $-NH_3^+$ group acts as a "structure-breaker."[43–47] These observations, in combination with recent MD simulations where the $-COO^-$ group accommodates more HBs with the proximal water molecules than $-NH_3^+$,[48,49] imply hydrophilic hydration is dominated by the strong hydration capacity of the $-COO^-$ group, with a relatively small contribution from the $-NH_3^+$ group. Based on the RDF of glycine aqueous solution, Campro[49] calculated the total number of HBs between glycine and water, 5.7, which is larger than our result n_{hyd}(gly) = 1.9; suggesting large fraction of the water molecules (i.e., 5.7 − 1.9 = 3.8 molecules) forms relatively weak HBs with the glycine solute, and thus, their reorientational dynamics are hard to distinguish from those of bulk water.

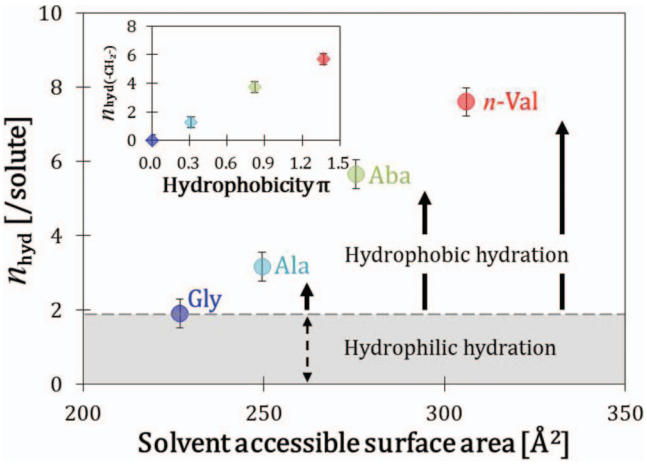

FIG. 5. Hydration number versus solvent accessible surface area (SASA) of amino acids. The gray area indicates hydrophilic hydration by the polar backbone. The inset shows the relationship between hydrophobicity (π) and hydrophobic hydration number.

If we assume the hydrophilic hydration number of the amino acid backbone is identical for all the amino acids, the number of hydrophobic hydration water trapped by the straight methylene side chains ($-CH_2-$) can be calculated by subtraction of the hydration number of the different amino acids, shown as solid bold arrows in Fig. 5. The inset in Fig. 5 shows the number of hydrophobic hydrated water and the hydrophobicity π of the amino acids as defined by Fauchère *et al.*[50] As the number of methylene side chains increases one by one, the hydrophobicity π becomes larger and larger, raising the number of hydrophobic hydration water by steps of 1.3–2.4. This number is similar to that obtained by the previous dielectric study, 1.9.[36] Assuming the van der Waals radius of carbon is 2.0 Å and of a water molecule is 1.4 Å, the average number of water molecules with access to the $-CH_2-$ surface was calculated to be 4.[20] Therefore two out of four water molecules in the first hydration shell of the methylene side chain are dynamically so retarded in the orientational direction that they are distinct from bulk water.

C. NHB water released from the HB network

In Fig. 4, $\tilde{\chi}_{fast}(\omega)$ of the glycine solution was found to be considerably larger than the other amino acids. This result stems from the significantly larger population of NHB water in the glycine solution. This supports the assumption that glycine solutes have a strong "destructuring" effect on the native HB network of water, releasing larger numbers of NHB water molecules from the HB network. To quantitatively determine the "destructuring" effect on the HB network, the mol concentration of the NHB bulk water C_{NHB} was calculated by Eq. (7),

$$C_{NHB} = \frac{\Delta\varepsilon^s_{fast}}{\Delta\varepsilon^w_{slow} + \Delta\varepsilon^w_{fast}} \frac{\rho_w}{M_w}. \quad (7)$$

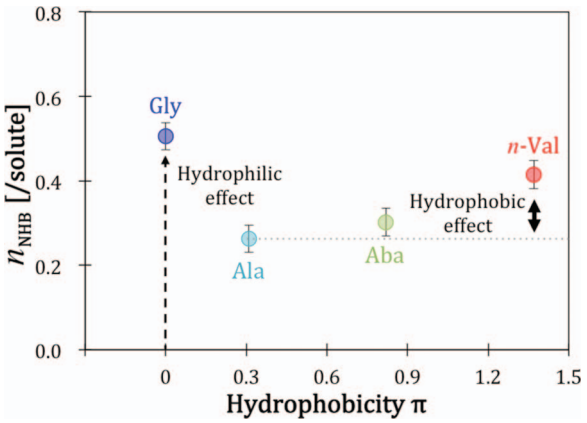

FIG. 6. Number of NHB water per a solute for each amino acid solution against hydrophobicity π.

Here, C_{HB} and C_{NHB} were related to the molar concentration of bulk water (C_{bulk}) by the equation, $C_{bulk} = C_{HB} + C_{NHB}$. Note that C_{NHB} considers both solute-induced NHB water and the native NHB water in the bulk water, which are located some distance from the solutes. Since the latter are not perturbed by the amino acid solutes, only the former will be directly associated with the "destructuring" effect of the amino acids. The number of NHB water molecules induced by a solute molecule (n_{NHB}) was determined by Eq. (8),

$$n_{NHB} = \frac{C_{NHB}}{C} - \frac{\Delta\varepsilon^{w}_{fast}}{\Delta\varepsilon^{w}_{slow} + \Delta\varepsilon^{w}_{fast}} \frac{C_{bulk}}{C}. \quad (8)$$

The first term on the right side is the total number of NHB water assigned per solute molecule and the second term denotes the native NHB water in the bulk phase. In this equation, it is assumed that the percentage of the NHB water in the bulk phase in the amino acid solution is equal to that in the distilled water. Then, the errors in n_{NHB} were determined in the same procedure based on the law of error-propagation, just as those in n_{hyd}.

C_{NHB} and n_{NHB} are listed in Table I. The larger n_{NHB} found for glycine solution (Fig. 6) is interpreted as glycine having a larger "destructuring" effect on the water HB network than that of the other three amino acids. Considering all the amino acids differ in the number of $-CH_2-$ groups they have, while maintaining exactly the same hydrophilic backbone, the change in n_{NHB} is assumed to be associated with the interaction between water molecules and the methylene groups. Noticeably stronger "destructuring" effect of glycine among amino acids has been also reported in various thermodynamical studies evidenced by a substantially large entropy,[51,52] and a negative enthalpic pair interaction coefficient.[53,54] The main reason for this "destructuring" effect may be ascribed to be the $-NH_3^+$ group in the amino acid backbone structure, which is known to be a structure-breaker,[55,56] as mentioned above.

Interestingly, an addition of a single methylene group to the hydrophilic amino acid backbone (i.e., alanine compared with glycine) significantly reduced n_{NHB}. From this result, it can be deduced that the "destructuring" effect of the hydrophilic backbone is significantly reduced by the first methylene group addition, which is consistent with TIP5P simulations performed by Godec *et al.*, who found that highly disordered HB structural components are more common around polar than apolar groups.[21] This trend seems to agree with the "iceberg" model proposed by Frank and Evans,[8] where the HB network around a hydrophobic regime is more structurally ordered like ice; implying a decreased NHB water population around hydrophobic groups. However, our results showed that n_{NHB} slightly but certainly increased with subsequent methylene group additions (Fig. 6), suggesting even hydrophobic groups have a weak "destructuring" effect. The rate of increase in n_{NHB} according to an addition of a single $-CH_2-$ group was larger than that in the SASA of the hydrophobic region, indicating that the increment in the hydrophobic moiety is not enough to explain the increasing tendency in Fig. 6. Thus, even hydrophobic groups, to some extent, have a "destructuring" effect on the native ordering of the water HB network, generating additional NHB water molecules. Therefore, our experimental result suggests a more nuanced version of the iceberg model: from the viewpoint of NHB water abundance, water molecules in the vicinity of the hydrophobic solute are actually more ordered than that around the hydrophilic region, but its ordering may not be as drastic as ice. Such an interpretation of the iceberg model is also evidenced by IR vibrational spectroscopy,[57] neutron scattering[17] and MD calculation,[58] which selectively probe the hydrocarbon/water interface.

D. Ordering of the tetrahedral HB network of water

In this section, we will focus on the tetrahedral HB network structure via measurements of the intermolecular stretching vibration mode of water $\tilde{\chi}_S(\omega)$. Theoretical studies [59–61] and THz measurements[29] have shown that the $\tilde{\chi}_S(\omega)$ mode around 5 THz is assigned to O ... O hindered translational motion in a "tetrahedral" HB environment. Since the tetrahedral HB network has a symmetric ordering, this vibration mode is originally Raman-active.[59] However, the intermolecular charge flux followed by the intermolecular stretching motion induces a dipolar movement, resulting in enhanced infrared-activity. Thus, a disordered tetrahedral HB network (i.e., distorted structure or large dynamical fluctuations in molecular positions) is likely to enhance the intermolecular stretching vibration $\tilde{\chi}_S(\omega)$.[29] On the other hand, when water adopts an ordered and symmetric tetrahedral coordination with smaller dynamical fluctuations, the $\tilde{\chi}_S(\omega)$ band becomes weaker, leading to an attenuation in the vibration strength (ΔV_S).

Fig. 7 shows the solute dependent vibration strength determined by the fitting procedure. For comparison, ΔV_S (water) $\times \beta$, where β is the mol ratio of "HB bulk + hydrated water" of the specific amino acid solution was compared to that of distilled water. In this comparison ΔV_S (water) $\times \beta$ is an analytical value taking into account water replacement by the solute molecules (water dilution effect). The assumption is that all the water molecules in the aqueous solution exhibit exactly the same stretching dynamics as pure water. Therefore, if ΔV_S is statistically equal

to analytical ΔV_S (water) $\times \beta$, it can be assumed that intermolecular stretching in the amino acid solutions is quite similar to that in distilled water. On the other hand, in case $\Delta V_S > \Delta V_S$ (water) $\times \beta$, we can consider that $\tilde{\chi}_S(\omega)$ mode is more activated in the solution due to solute–water interactions. As seen in Figure 7, the glycine aqueous solution had a significantly larger ΔV_S (left bar) than ΔV_S (water) $\times \beta$ (right bar). This is a direct indication that the tetrahedral HB network is more dynamical in the presence of glycine solute molecules. In the case of the other three amino acids, there was no such significant enhancement in ΔV_S; the values for ΔV_S and ΔV_S (water) $\times \beta$ overlapped within the range of error bars. This noticeable enhancement in ΔV_S for glycine solutions has been also found in other THz measurements,[62] and recently, Havenith and co-workers pointed out that the enhanced vibrational intensity was found only in glycine solutions, and not other amino acids such as alanine.[63] They combined THz spectroscopy with MD simulations, and used these to attribute the enhanced vibration mode around 5 THz to the strong stretching vibration between water and glycine (especially $-NH_3^+$ group in glycine).[42] Taking into account that as ΔV_S becomes larger the tetrahedral water coordination becomes more dynamical, their experimental results can be interpreted as follows: the tetrahedral coordination of water molecules around the $-NH_3^+$ group is dynamically disordered, leading to a larger vibration strength (ΔV_S). This interpretation is in line with the concept that $-NH_3^+$ groups act as a "structure-breaker," as predicted by thermodynamical studies.[55,56] While the addition of a methylene group $-CH_2-$ to glycine substantially lowered ΔV_S (Fig. 7), implying the $-CH_2-$ group retards the dynamical fluctuations of the water HB network. Further additions of $-CH_2-$ groups (i.e., Ala → Aba → *n*-Val) did not exhibit further significant decreases.

The bar graphs in Fig. 8 illustrate the resonant frequency (ω_S) and damping constant (γ_S) of the best-fitted results from Eq. (4). The resonant frequencies of the amino acids were not significantly different from that of distilled water, ω_S(water) = 5.22 THz. It is known that the resonant frequency of intermolecular stretching motion is correlated with average intermolecular distance.[64] This is because the shorter average HB distance stiffens the HB strength, which increases the HB stretching frequency.[65] Indeed, as water–water average distances shorten, (i.e., when liquid water is cooled), the water structure approaches an ice-like environment, where ω_S undergoes a blueshift.[66,67] On the other hand, ω_S was not significantly different among amino acid solutions we measured; irrespective of the number of the hydrophobic groups in the amino acid side chain. This result is inconsistent with the ice-like structure around the hydrophobic region as described by the "iceberg" model of Frank and Evans.[8] Thus, our results suggest the average HB distance in the first hydration shell (i.e., the hydrophilic solute–water distances and water–water distances surrounding hydrophobic surface) do not differ much from the HB distance in bulk water. This result is supported by RDF of various hydrophilic groups obtained by MD simulations, which showed the distance between hydrophilic solute and hydrated water is similar to the HB distance in bulk water.[68,69] Additionally, RDF studies around hydrophobic solutes also demonstrated that water–water distance in the hydrophobic hydration shell is also very close to that of bulk water at the same temperature.[17,22]

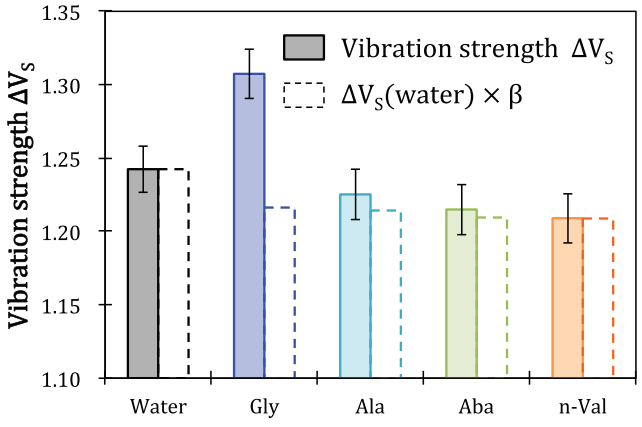

FIG. 7. (Left bar) Normalized vibration strengths ΔV_S with error spans (right bar) analytical oscillator strengths considering water molar fraction, ΔV_S (water) $\times \beta$, where β is the ratio of "HB bulk + hydrated water" in the amino acid solutions against that in the distilled water. The bars represent the analytical errors arisen in the least-square process.

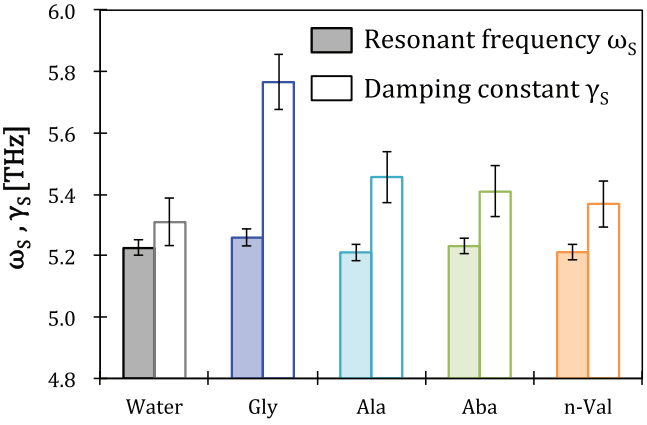

FIG. 8. (Left) Resonant frequency ω_S and (right) damping constant γ_S of distilled water and amino acid solutions with error spans. The bars represent the analytical errors arisen in the least-square calculation.

In contrast to the relatively consistent resonant frequency (ω_S), the damping constant γ_S was the largest in glycine, gradually decreasing as hydrophobicity increased (Fig. 8). Based on the water isotope effect on complex dielectric constants in the THz region, it has been experimentally shown that the damping constant γ_S and the order of water tetrahedrality is negatively correlated with each other.[29] In other words, a smaller damping constant reflects a more highly ordered tetrahedral HB network with uniform HB distances and angles. Therefore, γ_S provides a "static" picture of the tetrahedral ordering of water, such as the distribution of the HB distances and angles, while ΔV_S represents a "dynamical" aspect of water molecules in the HB network. From this standpoint, a significantly larger γ_S for glycine implies hydrophilic–water interactions that have a marginally disturbed tetrahedral structure in the HB network, and widening HB distances and angles. This observation is in agreement with the "structure-breaking" effect of the $-NH_3^+$ group with a more disordered native tetrahedral HB ordering around the

glycine surface. White and Jiang also came to a similar conclusion using *ab initio* MD simulation;[70] a decrease in tetrahedral order parameters q for glycine solutions. While not significant, the gradual drop in γ_S as further –CH_2– groups were added to the glycine base (Fig. 8) suggests hydrophobic methylene side chains do form an ordered and uniform tetrahedral HB network of water around them. Recent MD computational studies have shown that tetrahedrality is enhanced around hydrophobic groups,[22] because water molecules can form a more ordered arrangement than in the bulk water, avoiding the enthalpic penalty associated with a loss of water–water HBs. However, to discuss whether hydrophobic hydration water is more tetrahedral than bulk water or not is beyond the present study, since the hydrophilic amino acid backbone prevents us from isolating the γ_S of the hydrophobic hydration water.

IV. CONCLUSION

Changes in the dynamical structure of water molecules near hydrophobic groups were experimentally measured via changes in the broadband complex dielectric constants of aqueous amino acid solutions in the THz region. By examining changes in the above properties as straight methylene groups (–CH_2–) were added to a hydrophilic amino acid backbone we were able to separate out water–hydrophobic and water–hydrophilic interactions. The derived theoretical susceptibilities represent slow relaxation of HB bulk water $\tilde{\chi}_{slow}(\omega)$, fast relaxation of NHB bulk water $\tilde{\chi}_{fast}(\omega)$, intermolecular stretching of water $\tilde{\chi}_S(\omega)$, and libration of water $\tilde{\chi}_L(\omega)$. ATR measurement scheme contributed to precise data acquisition with small measurement errors, assuring the accuracy of the spectrum decomposition procedure.

Since the dielectric responses in the THz region reflect the relaxation dynamics of bulk water and that of hydrated water is negligibly small, the hydration number was determined from the reduction in the amount of bulk water. As a result, while the amino acid backbone has 1.9 hydrophilic hydration water molecules, our experimental results showed that each straight methylene group (–CH_2–) restrains approximately two hydrophobic hydration water molecules. Furthermore, the HB network of water around the hydrophobic region was experimentally examined in two ways: the population of the NHB water isolated from the HB network and the dynamical structure of water engaged in the tetrahedral HB network. The hydrophilic amino acid backbone was likely to "destructure" the HB network, producing more NHB water and distorting the tetrahedral HB arrangement, mainly due to the –NH_3^+ group. On the other hand, we found that an addition of hydrophobic –CH_2– side chain to the hydrophilic backbone pronouncedly orders the HB network with reducing the population of NHB water and forming less distorted tetrahedral HB network. Further addition of a single –CH_2– side chain did not exhibit more structuring effect, or if anything, tended to increase the population of the NHB water.

To summarize, water molecules around the hydrophobic groups were more ordered than those around hydrophilic ones: more dynamically restrained and less conformationally distorted. However, the degree of the ordering was not as extreme as the iceberg model of Frank and Evans,[8] which explained the unusually large entropy loss upon dissolution of hydrophobic solutes.[5] Rather, our results are consistent with a more "moderate" view of the iceberg model, in line with various previous simulations[22,23] and experiments.[13–15]

ACKNOWLEDGMENTS

We are grateful to Mr. Motoki Imamura and Mr. Akiyoshi Irisawa (ADVANTEST Corporation, Japan) for their technical supports. We also acknowledge Professor Garry John Piller (Graduate School of Agriculture, Kyoto University, Japan) for his help and useful discussions. Financial support was provided by Industry-Academia Collaborative R&D from Japan Science and Technology Agency (JST).

[1] K. A. Sharp, Curr. Biol. **1**, 171 (1991).
[2] H. I. Petrache, N. Gouliaev, S. Tristram-Nagle, R. Zhang, R. M. Suter, and J. F. Nagle, Phys. Rev. E **57**, 7014 (1998).
[3] L. Zídek, M. V. Novotny, and M. J. Stone, Nat. Struct. Mol. Biol. **6**, 1118 (1999).
[4] O. W. Howarth, J. Chem. Soc., Faraday Trans. **71**, 2303 (1975).
[5] W. Blokzijl and J. B. F. N. Engberts, J. Angew. Chem., Int. Ed. Engl. **32**, 1545 (1993).
[6] W. Kauzmann, Adv. Protein Chem. **14**, 1 (1959).
[7] N. T. Southall, K. A. Dill, and A. D. J. Haymet, J. Phys. Chem. B **106**, 521 (2002).
[8] H. S. Frank and M. W. Evans, J. Chem. Phys. **13**, 507 (1945).
[9] T. Head-Gordon, J. M. Sorenson, A. Pertsemlidis, and R. M. Glaeser, Biophys. J. **73**, 2106 (1997).
[10] N. Bjerrum, Science **115**, 385 (1952).
[11] G. Hummer, S. Garde, A. E. Garca, A. Pohorille, and L. R. Pratt, Proc. Natl. Acad. Sci. U.S.A. **93**, 8951 (1996).
[12] D. Laage, G. Stirnemann, F. Sterpone, R. Ray, and J. T. Hynes, Annu. Rev. Phys. Chem. **62**, 395 (2011).
[13] J. Qvist and B. Halle, J. Am. Chem. Soc. **130**, 10345 (2008).
[14] D. Laage, G. Stirnemann, and J. T. Hynes, J. Chem. Phys. B **113**, 2428 (2009).
[15] G. Stirneman, J. T. Hynes, and D. Laage, J. Chem. Phys. B **114**, 3052 (2010).
[16] Y. L. A. Rezus and H. J. Bakker, Phys. Rev. Lett. **99**, 148301 (2007).
[17] P. Buchanan, N. Aldiwan, A. K. Soper, J. L. Creek, and C. A. Koh, Chem. Phys. Lett. **415**, 89 (2005).
[18] M.-C. Bellissent-Funel, R. Sridi-Dorbez, and L. Bosio, J. Chem. Phys. **104**, 10023 (1996).
[19] D. W. Urry, S. Q. Peng, J. Xu, and D. T. McPherson, J. Am. Chem. Soc. **119**, 1161 (1997).
[20] M. Suzuki, J. Shigematsu, Y. Fukunishi, and T. Kodama, J. Phys. Chem. B **101**, 3839 (1997).
[21] A. Godec, J. C. Smith, and F. Merzel, Phys. Rev. Lett. **107**, 267801 (2011).
[22] N. Galamba, J. Phys. Chem. B **117**, 2153 (2013).
[23] N. Galamba, J. Phys. Chem. B **118**, 4169 (2014).
[24] P. Ball, Chem. Rev. **108**, 74 (2008).
[25] M. Chaplin, Nat. Rev. Mol. Cell Bio. **7**, 861 (2006).
[26] B. Bagchi, Chem. Rev. **105**, 3197 (2005).
[27] C. Ronne and S. R. Keiding, J. Mol. Liq. **101**, 199 (2002).
[28] H. Yada, M. Nagai, and K. Tanaka, Chem. Phys. Lett. **464**, 166 (2008).
[29] H. Yada, M. Nagai, and K. Tanaka, Chem. Phys. Lett. **473**, 279 (2009).
[30] T. Arikawa, M. Nagai, and K. Tanaka, Chem. Phys. Lett. **457**, 12 (2008).
[31] H. Hirori, K. Yamashita, M. Nagai, and K. Tanaka, Jpn. J. Appl. Phys. **43**, L1287 (2004).
[32] M. Nagai, H. Yada, T. Arikawa, and K. Tanaka, Int. J. Infrared Millimeter Waves **27**, 505 (2006).
[33] J. E. Bertie and Z. Lan, J. Chem. Phys. **105**, 8502 (1996).
[34] J. E. Bertie and H. H. Eysel, Appl. Spectrosc. **39**, 392 (1985).
[35] Y. Shi and L. Wang, J. Phys. D: Appl. Phys. **38**, 3741 (2005).
[36] T. Sato, R. Buchner, S. Fernandez, A. Chiba, and W. Kunz, J. Mol. Liq. **117**, 93 (2005).
[37] I. Rodríguez-Arteche, S. Cerveny, Á. Alegría, and J. Colmenero, Phys. Chem. Chem. Phys. **14**, 11352 (2012).

[38]S. Pal, S. Balasubramanian, and B. Bagchi, Phys. Rev. E. **67**, 061502 (2003).
[39]J. J. Moré, *Numerical Analysis* (Springer, Berlin, 1978).
[40]I. Ohmine, J. Phys. Chem. **99**, 6767 (1995).
[41]C. Cametti, S. Marchetti, C. M. C. Gambi, and G. Onori, J. Phys. Chem. B **115**, 7144 (2011).
[42]J. Sun, G. Niehues, H. Forbert, D. Decka, G. Schwaab, D. Marx, and M. Havenith, J. Am. Chem. Soc. **136**, 5031 (2014).
[43]K. Tamaki, Y. Ohara, H. Kurachi, M. Akiyama, and H. Odaki, Bull. Chem. Soc. Jpn. **47**, 384 (1974).
[44]G. C. Kreshek and L. Benjamin, J. Phys. Chem. **68**, 2476 (1964).
[45]H. Uedaira, Bull. Chem. Soc. Jpn. **50**, 1298 (1977).
[46]M. Ishimura and H. Uedaira, Bull. Chem. Soc. Jpn. **63**, 1 (1990).
[47]S. Okouchi, T. Moto, Y. Ishihara, H. Numajiri, and H. Uedaira, J. Chem. Soc., Faraday Trans. **92**, 1853 (1996).
[48]I. Wood, M. F. Martini, and M. Pickholz, J. Mol. Struc. **1045**, 124 (2013).
[49]M. G. Campo, J. Chem. Phys. **125**, 114511 (2006).
[50]J.-L. Fauchère, M. Charton, L. N. Kier, A. Verloop, and V. Pliska, Int. J. Pept. Protein Res. **32**, 269 (1988).
[51]A. L. Robinson, J. Chem. Phys. **14**, 588 (1946).
[52]C. H. Spink and M. Auker, J. Phys. Chem. **74**, 1742 (1970).
[53]B. Palecz, J. Therm. Anal. **54**, 257 (1998).
[54]B. Palecz, H. Piekarski, and S. Romanowski, J. Mol. Liq. **84**, 279 (2000).
[55]O. D. Bonner, J. M. Bednarek, and R. K. Arisman, J. Am. Chem. Soc. **99**, 2898 (1977).
[56]Y. Kameda, H. Ebata, T. Usuki, O. Uemura, and M. Misawa, Bull. Chem. Soc. Jpn. **67**, 3159 (1994).
[57]L. F. Scatena, M. G. Brown, and G. L. Richmond, Science **292**, 908 (2001).
[58]T.-M. Chang and L. X. Dang, J. Chem. Phys. **104**, 6772 (1996).
[59]N. Agmon, J. Phys. Chem. **100**, 1072 (1996).
[60]M. Sharma, R. Resta, and R. Car, Phys. Rev. Lett. **95**, 187401 (2005).
[61]J. Martí, J. A. Padro, and E. Guàrdia, J. Chem. Phys. **105**, 639 (1996).
[62]Y. Ogawa, L. Cheng, S. Hayashi, and K. Fukunaga, IEICE Electr. Express **6**, 117 (2009).
[63]G. Niehues, M. Heyden, D. A. Schmidt, and M. Havenith, Faraday Discuss. **150**, 193 (2011).
[64]D. A. Schmidt, Ö. Birer, S. Funkner, B. P. Born, R. Gnanasekaran, G. W. Schwaab, D. M. Leitner, and M. Havenith, J. Am. Chem. Soc. **131**, 18512 (2009).
[65]A. Lerbret, F. Affouard, P. Bordat, A. Hedoux, and M. Descamps, J. Non-Cryst. Solids **357**, 695 (2011).
[66]H. R. Zelsmann, J. Mol. Struct. **350**, 95 (1995).
[67]J. E. Bertie and S. M. Jacobs, J. Chem. Phys. **67**, 2445 (1977).
[68]Y. Tamai, H. Tanaka, and K. Nakanishi, Macromolecules **29**, 6750 (1996).
[69]S. L. Lee, P. G. Debenedetti, and J. R. Errington, J. Chem. Phys. **122**, 204511 (2005).
[70]A. White and S. Jiang, J. Phys. Chem. B **115**, 660 (2011).